Dynamic interactions between drops—a critical assessment

Rogerio Manica,[a] Evert Klaseboer[a] and Derek Y. C. Chan*[abc]

Received 21st April 2008, Accepted 21st May 2008
First published as an Advance Article on the web 10th June 2008
DOI: 10.1039/b806741d

Accurate measurements and modelling of time-dependent deformations of colliding liquid drops demonstrate the need to account for drop deformation and film drainage with appropriate initial and boundary conditions and reveal significant quantitative differences with the Stefan–Reynolds flat film model of drop coalescence.

Understanding the drop coalescence mechanism provides the essential foundations in effective control of polymer blending processes[1] and droplet reactors in microfluidic devices.[2] For over half a century, the coalescence stages of two liquid drops (or bubbles) have been visualised as the initial development of an increasing interaction zone between the drops as they approach and deform to trap an interstitial film of the dispersed phase of uniform thickness. This parallel or flat film is assumed to thin under the Stefan–Reynolds[3] drainage model until the two interfaces become sufficiently close together to come under the influence of van der Waals attraction. This attraction then amplifies thermal or capillary fluctuations which ultimately destabilise the film and lead to coalescence.[4] In spite of earlier observations based on interference methods, which indicated that the trapped film is not parallel,[5] the model remains in common use as the basis of further complex theoretical refinements.[6] However, the fundamental physical premise of this model is internally inconsistent and connection between the limited amount of experimental data[7] cited to justify this model and its extensions is often difficult to understand.

In this Communication, we report detailed optical interference measurements of time-dependent profiles of the trapped film between two drops that are driven together under well-defined initial and boundary conditions. The results are used to make a critical assessment of the accepted paradigm of the dynamic processes of drop approach, deformation and film drainage that lead to coalescence. The time-evolution of the film profiles, obtained from analysis of video recordings of interference fringes, differs significantly even in qualitative ways from the coalescence model described above. However, accurate quantitative predictions of all experimental results can be obtained with a model that treats drop deformations and time-varying hydrodynamic pressure distributions in the interstitial film in a mutually consistent fashion using standard lubrication theory coupled with the Young–Laplace equation at the drop–film interface. Furthermore, there is no evidence in the present experimental system that thermal or capillary fluctuations play a role in the coalescence process.

The experimental system was comprised of two identical glycerol half-drops with an undeformed radius $R = 1.52$ mm and interfacial tension $\sigma = 30$ mN m^{-1} formed as opposing protuberant drops from the ends of two sealed capillaries (3 mm diameter) in silicon oil with a contact angle $\theta = 90°$ at the capillary. Careful alignment of the capillary axes ensured head-on interactions. From rest at an initial separation h_{init}, the drops were driven together by propelling one capillary along the common axis towards the other at a constant velocity $V = 6.7$ μm s^{-1}. With the instant $t = 0$ set to be the time when the two drops would have touched if they did not deform, the drive stopped at $t_{\text{stop}} = 27$ s.

Variations of the profile of the silicone oil film between the glycerol drops were monitored by laser interferometry directed along the capillary axis using video recording of the changing fringe patterns. Full details of the experimental apparatus and methodologies have been given elsewhere.[8] Samples of the interference fringes produced by the drainage of the silicone oil film at different times are shown in Fig. 1 on the left hand side of each plot. The film between the drops continued to evolve after t_{stop} until they coalesced.

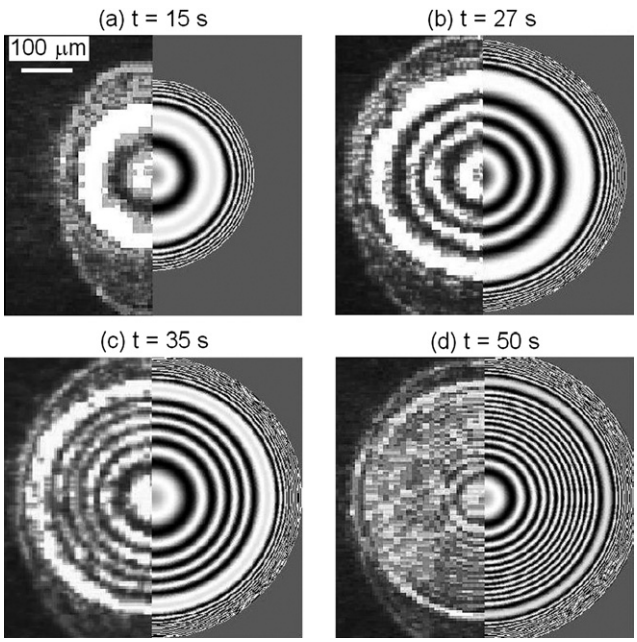

Fig. 1 Comparisons of experimental (left) and predicted (right) interference fringes produced by drainage of the silicone oil (Rhodorsil 47 V300, viscosity 0.3 Pa s) film between approaching glycerol drops (98.5% Rectapur, viscosity 1.0 Pa s) at times $t = 15$, 27, 35 and 50 s. The drops are driven together until $t_{\text{stop}} = 27$ s at constant velocity 6.7 μm s^{-1}.

[a]*Institute of High Performance Computing, 1 Science Park Road, 117528, Singapore. E-mail: manicar@ihpc.a-star.edu.sg; evert@ihpc.a-star.edu.sg; D.Chan@unimelb.edu.au; Fax: +65 6778 0522; Tel: +65 6419 1111*
[b]*Department of Mathematics, National University of Singapore, 117543, Singapore. E-mail: D.Chan@unimelb.edu.au*
[c]*Particulate Fluids Processing Centre, Department of Mathematics and Statistics, The University of Melbourne, Parkville, Victoria 3010, Australia. E-mail: D.Chan@unimelb.edu.au; Fax: +61 3 8344 4599; Tel: +61 3 8344 5556*

The intensity maxima at radial position r in a fringe pattern at a given time step or video frame can be converted to the local film thickness $h(r,t)$ using the Bragg equation for a fringe of order m: $h = m\lambda/2n$ where $\lambda = 632.8$ nm is the wavelength of the laser and $n = 1.41$ is the refractive index of the silicon oil. The results can be compared with a model that takes into account drop deformation due to the hydrodynamic pressure $p(r,t)$ in the draining silicone oil film treated as a Newtonian fluid with shear viscosity μ to give the thickness $h(r,t)$ between the deforming glycerol drops. The governing equations are:

$$\frac{\sigma}{2r}\frac{\partial}{\partial r}\left(r\frac{\partial h}{\partial r}\right) = \Delta P - p \tag{1}$$

$$\frac{\partial h}{\partial t} = \frac{1}{12\mu r}\frac{\partial}{\partial r}\left(rh^3\frac{\partial p}{\partial r}\right) \tag{2}$$

$$F(t) = 2\pi\int_0^\infty p(r,t)r\,\mathrm{d}r \tag{3}$$

where $F(t)$ is the instantaneous time-dependent force between the two drops. Eqn (1) follows from the augmented Young–Laplace equation that describes small axially symmetric deformations of the silicone film between the glycerol drops with a constant glycerol–silicone oil interfacial tension σ with $\partial h/\partial r \ll 1$. The drainage of the axially symmetric film as the drops approach is governed by eqn (2) which is derived from Stokes flow and lubrication theory. For later reference we call this the Stokes–Reynolds–Young–Laplace (SRYL) model of film drainage. Implicit in the formulation of eqn (2) is the assumption that the *no-slip* or *immobile interface* hydrodynamic boundary condition holds at the glycerol–silicone oil interface. The use of the *full-slip* or *fully mobile* boundary condition as suggested by theoretical analysis[9] of flow involving drops in similar geometries would overestimate the drainage rate when compared to experiments. As deformations are small compared to the undeformed drop radius, the Laplace pressure term ΔP can be approximated by $2\sigma/R$. Eqn (1) and (2) are to be solved in the inner region of the film $0 < r < r_{max}$. Detailed scaling arguments for the choice of r_{max} are given in detail elsewhere[10,11] but for the present work $r_{max} \approx 950$ μm is sufficient for numerical convergence. The initial condition for the model is $h(r,t = 0) = h_{init} + r^2/R$. The outer boundary condition at r_{max} that preserves the volume of the drops and obeys the constraint that the base of each drop that is anchored to the capillary is:[10,11]

$$\frac{\partial h}{\partial t} + \frac{\alpha}{2\pi\sigma}\frac{dF}{dt} = -V, \text{ at } r = r_{max} \tag{4}$$

where $\alpha = 2 + \ln(r_{max}^2/4R^2) + \ln[(1 + \cos\theta)/(1 - \cos\theta)]$, and θ is the contact angle of the drops at the capillary.[11] The contribution to the force integral in eqn (3) from $r > r_{max}$ is accounted for by extrapolating with the r^{-4} large r form of the pressure.[11] The equivalent of eqn (1)–(3) has been introduced earlier to study hydrodynamic effects and film deformation,[12] but appropriate initial and boundary conditions corresponding to eqn (4) were not available to facilitate direct quantitative comparison with experiments.

Film profiles extracted from experimental interference fringe patterns are compared to profiles predicted using the SRYL model in Fig. 2. The model profiles can also be used to generate interference fringes[13] and compare directly with the experimental fringes (right hand side of the plots in Fig. 1).

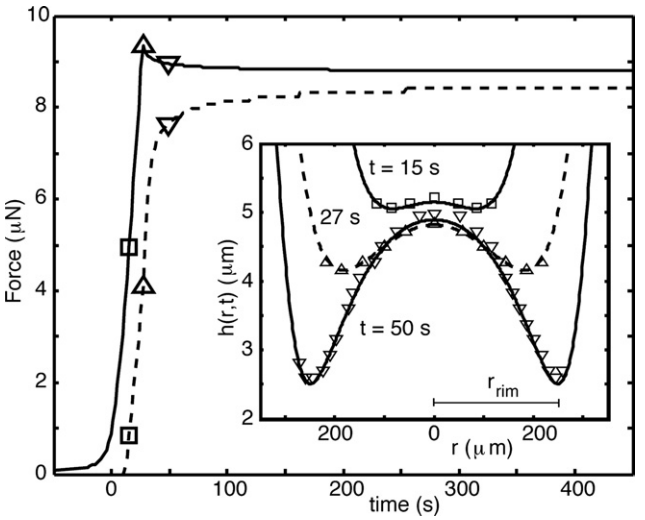

Fig. 2 The computed force $F(t)$ between the drops (—) as a function of time from the model given by eqn (1)–(4) and the force estimated using the formula $(2\sigma/R)\pi[r_{rim}(t)]^2$ from values of $r_{rim}(t)$ from the model (----), see Fig. 3. Inset: comparison of experimental and theoretical film profiles $h(r,t)$ at $t = 15$ s (□, —), 27 s (= t_{stop}) (△, ----) and at 50 s (▽, —). These three times are also marked on the force curves in the main figure.

We note the axial symmetry of the experimental profiles and the development of the characteristic hydrodynamic dimple with the associated formation of a rim of minimum separation h_{rim} at $r = r_{rim}$ that arises when the hydrodynamic pressure in the film exceeds the Laplace pressure of the drops. The hydrodynamic force $F(t)$ between the two drops calculated according to eqn (3) is also shown in Fig. 2. We see that while the capillaries are driven together at constant velocity during $t < t_{stop}$, the force increases monotonically. After the capillary stopped, the film continues to evolve under a constant force regime. Therefore the results after $t > t_{stop}$ are relevant to situations when drops are driven together under constant force conditions such as under the influence of gravity. For instance, in the present experiment, the hydrodynamic dimple continues to develop in size under constant force conditions during $t > t_{stop}$ (see also Fig. 3).

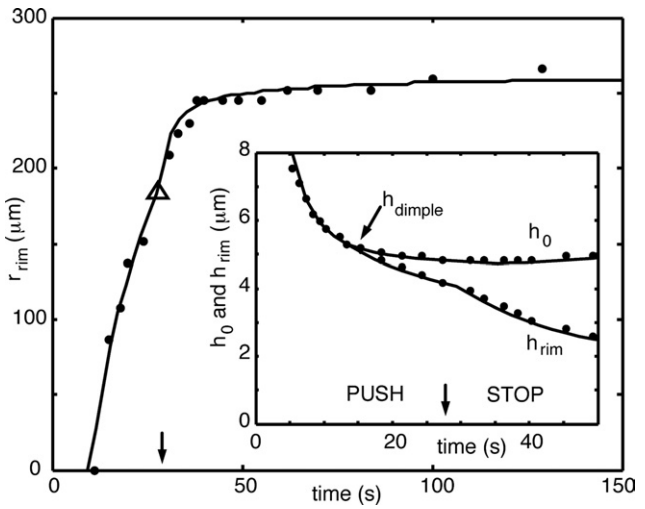

Fig. 3 Time variations of r_{rim}, the position of the thinnest part of the film. The time t_{stop} is marked by △ and the arrows. Inset: close-up view of Fig. 4 around the time when the hydrodynamic dimple first develops.

At $t = 12$ s, the hydrodynamic dimple forms and the minimum film thickness is found on a circular rim of radius $r_{rim} > 0$ rather than at $r = 0$. As the dimple develops, the film radius r_{rim} also increases rapidly (Fig. 3) before attaining a plateau value some time after the capillary has stopped. In the Stefan–Reynolds parallel film model, the force $F_{SR}(t)$ between drops is often estimated by: $F_{SR}(t) = \Delta P\pi[r_{rim}(t)]^2 = (2\sigma/R)\,\pi[r_{rim}(t)]^2$ where $r_{rim}(t)$ is found by solving eqn (1)–(4). A direct comparison between this expression for the force and the force computed by eqn (3) is given in Fig. 2. At $t = t_{stop}$ this approximate formula underestimates the actual force by a factor of 2—assuming r_{rim} can be obtained from experiments or by some other means. An important observation concerning the Stefan–Reynolds parallel film model is its internal inconsistency. According to the Young–Laplace equation, a flat interface implies a constant pressure difference between the interior of the drops and the film throughout the parallel flat film and yet, the parallel film model is used to calculate variations of the hydrodynamic pressure in the radial direction that controls the thinning of the parallel film. Furthermore, 80% of the force calculated by eqn (3) comes from the interval $0.5r_{rim} < r < \infty$ of the integral. Thus it is the part of the film where the thickness varies rapidly around the rim that makes the most quantitative contribution to the total force. Consequently the common practice of measuring the film thickness around $r = 0$ may not yield useful information about the dynamical properties of interacting drops.

To further illustrate the above observation, we show the time-evolution of film thickness at the centre of the film: $h_o(t) = h(0,t)$ and at the rim position $h_{rim}(t) = h(r_{rim},t)$ in Fig. 4. Note that after the capillary has stopped moving ($t > t_{stop} = 27$ s), $h_o(t)$ actually increases slightly with a shallow maximum at $t \approx 90$ s before decreasing very slowly to a value of around 4.8 μm at $t \approx 250$ s. On the other hand while $h_{rim}(t)$ decreases rapidly from around 5 μm at the formation of the dimple at $t \approx 12$ s to around 1.5 μm at $t \approx 100$ s, it then decreases slowly to just under 1 μm at $t \approx 250$ s. All such drainage behaviour is due entirely to the coupling between hydrodynamic effects and interfacial deformations because surface forces (such as van der Waals attraction) are negligible at this range of film thickness.

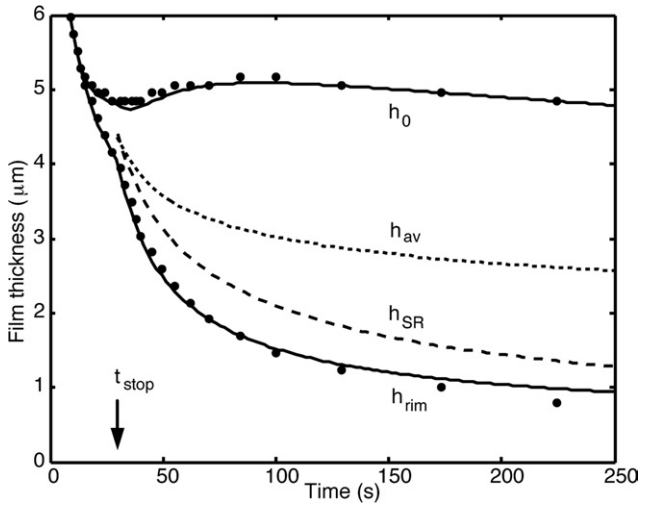

Fig. 4 Time variations of $h_o = h(r = 0,t)$ and $h_{rim} = h(r_{rim},t)$. The dimple first develops at $t = 12$ s. Note that h_o increases slightly after t_{stop} with a shallow maximum at $t \approx 90$ s. A close-up view around the onset of the hydrodynamic dimple is given in the inset of Fig. 3. Results of the thickness $h_{SR}(t)$ is from the Stefan–Reynolds parallel film model, eqn (5) assuming a constant film radius $a = 250$ μm and a constant force $F = 9$ μN (see text) and the average thickness $h_{av}(t)$, eqn (6) are also shown.

We can compare the experimental film thinning results with the Stefan–Reynolds parallel film model with uniform film thickness $h_{SR}(t)$ and effective film radius $a(t)$ thinning under an applied force $F(t)$ governed by the equation:[6]

$$\frac{dh_{SR}}{dt} = -\frac{2h_{SR}^3 F}{3\pi\mu a^4} \tag{5}$$

To solve this equation for the uniform film thickness $h_{SR}(t)$, it is necessary to specify the film radius $a(t)$ and the applied force $F(t)$. We see from Fig. 2 that for $t \geq 30$ s, $r_{rim}(t)$ has attained a constant value of 250 μm which we will take as the constant film radius a, while the force F (see Fig. 1) has reached the constant plateau value of 9 μN. With these values, the evolution of the Stefan–Reynolds parallel film can be found by solving eqn (5) analytically with the initial condition: $h_{SR}(t = 30\text{ s}) = 4.5$ μm and the result is plotted in Fig 4. Also shown in Fig. 4 is an average film thickness $h_{av}(t)$ defined by:

$$h_{av}(t) \equiv \frac{2}{r_{rim}(t)^2}\int_0^{r_{rim}(t)} h(r,t)r\mathrm{d}r \tag{6}$$

Traditional experiments measure the thickness at the centre of the film $h_o(t) = h(0,t)$ while it is the film thickness at the rim $h_{rim}(t) = h(r_{rim},t)$ that determines film stability and the onset of coalescence. Furthermore, the Stefan–Reynolds parallel film model requires additional information about the film radius and the force before it can be solved. Since we have demonstrated here that the entire film thickness $h(r,t)$ can be measured accurately as a function of position and time it is clear that film drainage theories based on a parallel film paradigm are unable to provide quantitatively informative results. On the other hand, the SRYL model can predict film evolution very accurately without any adjustable parameters until the point of film rupture. After film rupture, a small bridge forms between the two coalescing drops. The expansion of the lateral dimension of this liquid bridge as the two drops combine is an extremely rapid event (compared to the approach to film rupture considered here) and is governed by the competition between interfacial tension and viscosity.[14]

In summary, we observe that:

- the spatio-temporal evolution of the trapped film between drops deforming under hydrodynamic interactions can be measured very accurately with interferometric techniques
- all details of the experimental results are in quantitative agreement with the Stokes–Reynolds–Young–Laplace (SRYL) model that treats drop deformation and film drainage in a consistent manner without adjustable parameters
- experimental results are consistent with the no-slip, immobile interface hydrodynamic boundary condition which may be attributable to the presence of surface active impurities in the system despite the fact that the experiments were performed under 'clean' conditions
- the present experimental results and predictions of the SRYL model are consistent with earlier studies of dynamic deformations of a mercury drop moving relative to a mica surface,[15–19] atomic force microscope measurements of dynamic forces between oil drops in

aqueous electrolytes,[20–22] between an oil drop and a solid particle[23] and between a bubble and a mica surface[24]

• the counter-intuitive behaviour of $h(0,t)$ actually increases shortly after the capillary has ceased being driven is also observed in drop–solid interactions[15,18]

• the Stefan–Reynolds parallel flat film model and its subsequent modifications are not able to give quantitative or qualitative accounts of the film drainage process apart from being a broad indicator of film thickness

• coalescence of dimpled drops occurs at the rim of the film at r_{rim} either when h_{rim} becomes sufficiently small for van der Waals attraction to rapidly accelerate the decrease in local film thickness[17] or when impurity particles that may be trapped at the interface trigger film rupture if the film becomes sufficiently thin at the rim

• capillary waves or thermal fluctuations of the entire parallel interface are unlikely to be the trigger mechanism for coalescence in dimpled films because of hydrodynamic dampening and surface tension stabilisation[18,20]

• the dimpling phenomenon is universal[9] and dimpling of driven drops occurs at the characteristic separation

$$h_{dimple} \approx cR(\mu V/\sigma)^{1/2}$$

where c is a constant that varies with a weak dependence on the contact angle θ and the capillary number ($Ca = \mu V/\sigma$) ranging from 0.4 for low Ca numbers ($Ca \approx 1 \times 10^{-10}$) to 0.7 for $Ca \approx 1 \times 10^{-4}$.

DYCC is a Visiting Professor at the National University of Singapore and an Adjunct Professor at the Institute of High Performance Computing. The experimental results were obtained by EK at the 'Institut de Mécanique des Fluides/Ecole National d'Ingénieurs de Génie Chimique' in Toulouse (France).

Notes and references

1 J. J. Elmendorp, *Mixing in Polymer Processing*, ed. C. Rauwendaal, Marcel Dekker, New York, 1991.
2 G. M. Whitesides, *Nature*, 2006, **442**, 368.
3 J. Stefan, *Sitzungsber. Akad. Wiss. Wien, Math. Naturwiss. Kl., Abt. 2*, 1874, **69**, 713; O. Reynolds, *Philos. Trans. R. Soc. London*, 1886, **A177**, 157.
4 See for example: G. E. Charles and S. G. Mason, *J. Colloid Sci.*, 1960, **15**, 236; Thin liquid films: fundamentals and applications, *Surfactant Science Series*, ed. I. B. Ivanov, M. Dekker, New York, 1988, vol. 29.
5 B. V. Deryaguin and M. Kussakov, *Acta Physicochim. URSS*, 1939, **10**, 25.
6 For recent reviews of the parallel film model and modifications, see: J. E. Coons, P. J. Halley, S. A. McGlashan and T. Tran-Cong, *Adv. Colloid Interface Sci.*, 2003, **105**, 3; J. E. Coons, P. J. Halley, S. A. McGlashan and T. Tran-Cong, *Colloids and Surfaces A: Physicochem. Eng. Aspects*, 2005, 263, p. 197.
7 B. P. Radoev, A. D. Schelduko and E. M. Manev, *J. Colloid Interface Sci.*, 1983, **95**, 254; E. Manev, R. Tsekov and B. Radoev, *J. Dispersion Sci. Technol.*, 1997, **18**, 769.
8 E. Klaseboer, J. Ph. Chevaillier, C. Gourdon and O. Masbernat, *J. Colloid Interface Sci.*, 2000, **229**, 274.
9 S. G. Yiantsios and R. H. Davis, *J. Fluid Mech.*, 1990, **217**, 547.
10 S. L. Carnie, D. Y. C. Chan, C. Lewis, R. Manica and R. R. Dagastine, *Langmuir*, 2005, **21**, 2912.
11 R. Manica, J. N. Connor, R. R. Dagastine, S. L. Carnie, R. G. Horn and D. Y. C. Chan, *Phys. Fluids*, 2008, **20**, 032101.
12 C.-Y. Lin and J. C. Slattery, *AIChE J.*, 1982, **28**, 147.
13 M. Born and E. Wolf, *Principles of Optics*, Cambridge University Press, Cambridge, 7th edn, 1999.
14 D. G. A. L. Aarts, H. N. W. Lekkerkerker, H. Guo, G. H. Wegdam and D. Bonn, *Phys. Rev. Lett.*, 2005, **95**, 164503.
15 J. N. Connor and R. G. Horn, *Faraday Discuss.*, 2003, **123**, 193.
16 L. Y. Clasholm, J. N. Connor, O. I. Vinogradova and R. G. Horn, *Langmuir*, 2005, **21**, 8243.
17 R. Manica, J. N. Connor, S. L. Carnie, R. G. Horn and D. Y. C. Chan, *Langmuir*, 2007, **23**, 626.
18 R. Manica, J. N. Connor, L. Y. Clasohm, S. L. Carnie, R. G. Horn and D. Y. C. Chan, *Langmuir*, 2008, **24**, 1381.
19 D. Y. C. Chan, O. Manor, J. N. Connor and R. G. Horn, *Soft Matter*, 2008, **4**, 471.
20 S. L. Carnie, D. Y. C. Chan, C. Lewis, R. Manica and R. R. Dagastine, *Langmuir*, 2005, **21**, 2912.
21 R. R. Dagastine, R. Manica, S. L. Carnie, D. Y. C. Chan, G. W. Stevens and F. Grieser, *Science*, 2006, **313**, 210.
22 G. B. Webber, S. A. Edwards, G. W. Stevens, F. Grieser, R. R. Dagastine and D. Y. C. Chan, *Soft Matter*, 2008, **4**, 1270.
23 G. B. Webber, R. Manica, S. A. Edwards, S. L. Carnie, G. W. Stevens, F. Grieser, R. R. Dagastine and D. Y. C. Chan, *J. Phys. Chem. C*, 2008, **112**, 567.
24 O. Manor, I. U. Vakarelski, X. Tang, S. J. O'Shea, G. W. Stevens, F. Grieser, R. R. Dagastine and D. Y. C. Chan, *Phys. Rev. Lett.*, submitted LR11119.